Research Article

RPTEC/TERT1 Cells Form Highly Differentiated Tubules When Cultured in a 3D Matrix

Philipp F. Secker[#], Lisanne Luks[#], Nadja Schlichenmaier and Daniel R. Dietrich

Human and Environmental Toxicology, Department of Biology, University of Konstanz, Konstanz, Germany

Summary

The proximal tubule is the primary site for renal solute reabsorption and secretion and thus a main target for drug-induced toxicity. Current nonclinical methods using 2D cell cultures are unable to fully recapitulate clinical drug responses mainly due to limited *in vitro* functional lifespan. Since extracellular matrices are known to be key regulators of cell development, culturing cells on classic 2D plastic surfaces inevitably results in loss of differentiation. Hence, 3D models of the human proximal tubule that recapitulate the *in vivo* morphology would allow for improved drug screening and disease modeling. Here, the development and characterization of a 3D proximal tubule model using RPTEC/TERT1 cells is presented. RPTEC/TERT1 cells self-assembled in matrigel to form highly differentiated and stable 3D tubular structures characterized by a branched network of monolayered cells encircling a cell-free lumen, thus mimicking the proximal tubule. *In vitro* tubuli resembled the polarity of a proximal tubule epithelium as indicated by polar expression of Na^+/K^+-ATPase and ZO-3. Furthermore, 3D cultured RPTEC/TERT1 cells showed overall increased mRNA expression of xenobiotic transporters, e.g., OCTs and MATEs and *de novo* expression of OAT3 when compared to cultures on plastics or membrane inserts. Finally, this model was used to assess delayed cisplatin-induced nephrotoxicity and demonstrated increased sensitivity when compared to 2D culture. Thus, the easy-to-use model described here may prove to be useful for mechanistic investigations, e.g., in discovery of compounds interfering with tubule formation, differentiation and polarization, as well for the detection and understanding of pharmaceutical induced nephrotoxicity.

Keywords: nephrotoxicity, *in vitro*, cisplatin, 3D cell culture, kidney

1 Introduction

Toxicology still heavily relies on animal experiments to predict adverse effects of drugs and chemicals in a human population. However, translatability of rodent findings towards the human situation is known to be often very poor (Hackam and Redelmeier, 2006; Leist and Hartung, 2013; Matthews, 2008; Olson et al., 2000; van der Worp et al., 2010), potentially resulting in undetected adverse effects (false negatives) or loss of valuable compounds due to species-specific side effects (false positives) (Hartung, 2009). Currently, chances of a drug candidate entering clinical phase I to be marketed are as low as 7% (Bunnage, 2011) and safety issues or lack of pharmacological efficacy are major reasons (Kola and Landis, 2004) revealed late during development despite extensive nonclinical studies.

Together with ethical considerations, e.g., the 3R (reduce, replace, refine) principle of animal testing (Russell and Burch, 1959), these disenchanting numbers have boosted the development of alternative, human cell-based test methods. In theory, the use of human cells overcomes the burden of translating results obtained from animal experiments to humans. In practice, however, results obtained from *in vitro* toxicology studies were often more than disappointing. For instance, one comprehensive study by Lin and Will with hundreds of either hepatotoxic, cardiotoxic or nephrotoxic compounds and three frequently used cell lines originating from the three organs found that only 5% of compounds exhibited differential toxicity and – even worse – in case of a differential response, the most sensitive cell line did not necessarily match with the most susceptible organ (Lin and Will, 2012).

[#] contributed equally

Received October 18, 2017;
Accepted December 1, 2017;
Epub December 2, 2017;
doi:10.14573/altex.1710181

This is an Open Access article distributed under the terms of the Creative Commons Attribution 4.0 International license (http://creativecommons.org/licenses/by/4.0/), which permits unrestricted use, distribution and reproduction in any medium, provided the original work is appropriately cited.

It is evident that the lack of specificity frequently observed in *in vitro* studies is often due to a lack of sensitivity in the target cell line, being poorly differentiated and thereby compromising *in vitro* to *in vivo* extrapolations (Wilmer et al., 2016). Most cells of the human body that carry out specific functions are either fully differentiated or under proliferation arrest. This is quite contrary to the situation of the cell *in vitro*, where proliferation is required to expand cultures and to obtain considerable cell numbers. However, cellular proliferation and differentiation are in fundamental conflict to each other. Thus, *in vitro* toxicologists now mainly focus on development of highly differentiated cell lines with the aim to establish cell lines exhibiting comparable functionality to their *in vivo* counterparts (Alépée et al., 2014). Extracellular matrices are known to be key regulators of cell development and tissue phenotype (Bissell et al., 2002; Astashkina et al., 2012a), thus culturing cells on classic 2D plastic surfaces inevitably results in loss of differentiation. Hence, 3D models of various cell types have been shown to dramatically increase differentiation of cells towards, e.g., hepatocytes (Dunn et al., 1991; Tostões et al., 2011; Tuschl et al., 2009; Zeilinger et al., 2011), skin-related cell types (Itoh et al., 2013; Roguet et al., 1994), nervous system (Lu et al., 2012; Smirnova et al., 2016) and intestinal cells (Grabinger et al., 2014; Sato et al., 2009). Thereby, 3D models help to recapitulate the tissue-specific morphology and allow for improved pharmacology and toxicology testing.

The renal proximal tubule epithelial cells (RPTECs) are primarily responsible for renal solute reabsorption and metabolism end-product excretion. Therefore, RPTECs express multiple transporters with broad substrate specificities also enabling uptake and excretion of xenobiotics. About one third of the top 200 prescribed drugs undergoes renal elimination and 90% of them are actively secreted into the urine, involving cellular transport processes (Morrissey et al., 2013). Anions are taken up at the basolateral membrane primarily by organic anion transporter (OAT) 1 and 3 and secreted at the apical membrane by the multidrug resistance proteins (MRP) 2 and 4 (Masereeuw et al., 1999), while cations are mainly taken up by organic cation transporter (OCT) 2 and are eliminated by multidrug and toxin extrusion proteins (MATE) 1 and 2K (Biermann et al., 2006; Cetinkaya et al., 2003; Sauzay et al., 2016) and P-glycoprotein (P-gp). Consequently, RPTECs experience high intracellular drug concentrations, potentially resulting in nephrotoxicity. Maintaining functional expression of these transporters *in vitro* is key for the successful prediction of a drug's nephrotoxic potential. However, to date, there is no continuous cell line available that functionally reflects the major proximal tubule transport processes. Moreover, even primary kidney cells lose functional transport already within hours or days in culture (Heussner and Dietrich, 2013; Tiong et al., 2014).

One promising cell model is the human RPTEC/TERT1 cell line originating from a male donor and being immortalized by telomerase overexpression (Wieser et al., 2008). The RPTEC/TERT1 cell line maintains many differentiation hallmarks, e.g., tight junction formation, stable transepithelial electrical resistance and vectorial cation transport via the OCT/MATE axis (Aschauer et al., 2015a). Conversely, functional uptake of anions via OATs and vectorial anion secretion could not be shown under standard culture conditions (Aschauer et al., 2015a). In conjunction with the latter findings and the fact that the RPTEC/TERT1 cell line maintained many of the crucial transporters under routine culturing conditions, it was hypothesized that improvement of culture conditions, e.g., providing an extracellular matrix environment, could result in a more differentiated phenotype and possibly in a gain of function such as anion transport. Hence, a three-dimensional (3D) matrigel sandwich culture was developed for RPTEC/TERT1. Under the latter conditions, RPTEC/TERT1 cells autonomously formed a network of tubular structures composed of single-layered cells. These cells were connected by tight junctions and were highly polarized with an apical membrane forming microvilli and a basolateral membrane that stained positively for Na^+/K^+-ATPase. This sandwich culture also resulted in a near *in vivo* like morphology, and in addition, presented a substantial degree of differentiation as indicated by increased mRNA expression of many transporters and brushborder markers. Finally, the sensitivity comparison of routine 2D and the novel 3D sandwich culture of RPTEC/TERT1 toward delayed cisplatin nephrotoxicity demonstrated a higher sensitivity of the sandwich culture.

2 Materials and methods

Chemicals and solutions

If not stated otherwise, all chemicals and solutions were purchased from Sigma-Aldrich, Germany.

Cell culture

The RPTEC/TERT1 cell line was obtained from Evercyte GmbH, Austria. RPTEC/TERT1 cells were cultured in a 1:1 mix of DMEM no glucose (Thermo Scientific) and Ham's F12 (Thermo Scientific), containing 5 mM glucose final and supplemented with 2 mM GlutaMAX (Thermo Scientific), 5 µg/ml insulin (Sigma, #I1882), 5 µg/ml transferrin (Sigma, #T2252), 10 ng/ml epidermal growth factor (Sigma, #E9644), 36 ng/ml hydrocortisone, 5 ng/ml sodium selenite, 100 U/ml penicillin and 100 µg/ml streptomycin. When cultured on plastic (2D), cells were seeded at 30% density into 6-well plates and grown either for 24 h (proliferating cells) or for at least 14 days (differentiated cells). When cells were cultured on PET Transwell® inserts (2.5D) with 0.4 µm pore size (Corning), they were seeded at 100% density and differentiated for at least 14 days. For 3D culture, RPTEC/TERT1 cells were seeded in between two layers of growth factor-reduced, phenol red-free Matrigel® (Corning, #356231) in a 96-well. The lateral wall of the 96-well was coated with heat-sterilized silicon grease using a pipette tip to avoid meniscus formation of matrigel. The well was coated with 35 µl matrigel and 70,000 cells were seeded onto the matrigel layer after the latter polymerized for 30 min at 37°C. After 16 h, cells were attached and formed branched tubular structures. Subsequently, the medium was removed and cells were capped with 25 µl matrigel per well. After polymerization of

the matrigel, 150 µl medium was added per well. Cells were cultured at 37°C with 5% CO_2 and medium was renewed every second or third day. 3D cultures were grown for at least 21 days before initiating experiments and morphology was assessed using an inverted microscope (ECLIPSE TS100/ TS100-F, Nikon).

Glucose quantification
Glucose content in cell culture medium was quantified enzymatically using the glucose oxidase (GOD), peroxidase (POD) coupled reaction. 10 µl sample was mixed with 90 µl reaction mix containing 100 U/ml GOD (Sigma, #G2133), 0.25 U/ml POD (Sigma, #P8250) and 1.5 mg/ml ABTS (Sigma, #I1882) in 0.1 M Na_2HPO_4 pH 6.5 followed by incubation for 40 min at room temperature. Afterwards, absorption at 420 nm was measured using a microplate reader (M200Pro, Tecan) and glucose content was calculated according to a D-glucose calibration curve (0-2 mM). Cellular glucose consumption was calculated by subtracting the remaining glucose content in conditioned medium from the content of fresh medium followed by normalization to exposure time and seeded cell number.

Lactate quantification
Lactate secreted into cell culture medium was quantified enzymatically using a microplate reader as published by Limonciel et al. (2011) without modifications. The amount of lactate was normalized to exposure time and seeded cell number.

Immunocytochemistry
For immunocytochemistry experiments, cells were cultured in Nunc™ Lab-Tek™ chamber slides (Fisher Scientific, #10507401) and differentiated for at least 21 days. Prior to staining, cells were washed 15 min in ice-cold PBS-EDTA as described by Lee et al. (2007). Then, cells were fixed for 30 min with 4% PFA/ 0.5% Triton-X 100 and blocked for 1 h in 1% bovine serum albumin in PBS. The following primary antibodies were incubated over night at 4°C: mouse anti-acetylated tubulin (1:100, Sigma-Aldrich, #T7451), rabbit anti-ZO-3 (1:500, Cell signaling, #3704), mouse anti-Na+/K+-ATPase (1:50, Santa Cruz, #sc-21712). After washing three times for 20 min in PBS, secondary antibodies were incubated for 2 h at room temperature (1:500, Alexa Fluor 488, goat anti-rabbit, #A-11008; Alexa Fluor 532 goat anti-mouse, #A-11002; Alexa Fluor 647 goat anti-rabbit, #A-21244; Thermo Fisher). After washing, nuclei were stained with Hoechst 33342 for 10 min. Then, the chamber was detached, excessive matrigel was carefully removed using a scalpel, and 3D structures were mounted using fluorescence mounting medium (Dako, #S3023) and covered with a glass coverslip.

Confocal microscopy
Cells were imaged using a point laser scanning confocal microscope LSM 880 (Zeiss) equipped with a 40x/1.4 Plan-Apochromate oil immersion objective and ZEN software. Confocal sections of 0.5 µm thickness were collected and a refractive index correction of 0.876 was applied to all images. Multiple fluorophores were imaged via sequential scanning. All pictures are representative for at least three independent experiments. Brightness/contrast of images was enhanced for display using (Fiji Is Just) ImageJ software. No background correction was applied.

Electron microscopy
Differentiated tubules were transferred into a multi-well plate and fixed at 4°C for 90 min in 1.9% formaldehyde, 3.75% glutardialdehyde, 0.045% picric acid, 0.045% $CaCl_2$ in 0.1 M HEPES. After washing, tissue was stained using 1% OsO_4 (Serva, #31253.01) for 90 min at 4°C and dehydrated in 30% and 50% ethanol for 10 min at 4°C. After en-bloc staining with uranyl acetate over night at 4°C, tubules were dehydrated (70-100% ethanol), embedded in ethanol:Spurr (3:1) solution for 30 min followed by an ethanol:Spurr (1:1) solution for 90 min and another 150 min in ethanol:Spurr (1:3) and subsequent overnight incubation in pure Spurr (Sigma, #EM0300). After incubation for 4.5 h at 40°C, tissue was flat-embedded and polymerized at 65°C for 48 h. Subsequently, 50 nm sections were cut using a Leica UC7 ultramicrotome. For contrast filling, sections were stained for 90 min in lead citrate and analyzed using the transmission electron microscope Zeiss EM Omega (80kV).

Quantitative real-time PCR
Total RNA of 2D and 3D samples was isolated according to manufacturer's instructions using the peqGOLD Total RNA Kit (VWR Peqlab, #732-2870) and the ReliaPrep RNA Tissue Miniprep System (Promega, #Z6110), respectively. For 3D samples, homogenates of 10 technical replicates were pooled. Reverse transcription was performed using the peqGOLD cDNA Synthesis Kit H Plus (VWR, #PEQL03-2041) following the manufacturer's instructions. Quantitative real-time PCR was performed in duplicate with 1:5 diluted cDNA and the KAPA SYBR FAST Master Mix (2x) Universal (VWR, #KK4600) in the CFX Connect Real-Time PCR Detection System (Bio-Rad). Primer sequences are listed in Table S1[1]. Expression of target genes was normalized to mean expression of three reference genes (ACTB, HPRT1, RPL13A). Values obtained for the different cultivation conditions were further normalized to expression in 3D cultures.

Uptake assays
For uptake assays, cells were cultured in Nunc™ Lab-Tek™ chamber slides (Fisher Scientific, #10507401) and differentiated for at least 21 days. Cells were incubated with 10 µM 4-(4-(dimethylamino)styryl)-N-methylpyridinium iodide (ASP^+) (Life Technologies) or 40 µM Lucifer yellow (LY) (Sigma-Aldrich) for 1, 24 or 48 h. Then, cells were stained with Hoechst 33342 and fixed for 30 min with 4% PFA without detergent. Cells were mounted, covered with a glass coverslip

[1] doi:10.14573/altex.1710181s

and imaged immediately using confocal microscopy (ASP^+: excitation: 477 nm, emission: 557 nm; LY: excitation: 425 nm, emission: 538 nm). Note that different laser power settings were used for ASP^+ (0.2%) and LY (35%) uptake visualization. For quantification of signal intensities within cells and lumen, fluorescence intensity of 15 randomly selected regions of interest (each 1 μm^2 size) was analyzed using the ImageJ software.

Resazurin assay

Resazurin reduction was used to quantify cellular viability. After cell treatment, medium was exchanged for fresh medium containing 45 µM resazurin followed by incubation at 37°C for 1 h. Medium was transferred to a black microplate and resorufin fluorescence was measured at 530 nm excitation, 590 nm emission. Viability was expressed as percent of non-treated cells.

LDH leakage assay

Lactate dehydrogenase (LDH) leakage into the cell culture medium was quantified as a cytotoxicity endpoint (loss of cell integrity). 20 µl of cell culture supernatant was mixed with 180 µl LDH reaction solution containing 1.25 mM NADH and 3.1 mM sodium pyruvate in 25 mM potassium phosphate buffer pH 7.5. Change in absorption of NADH at 340 nm was monitored every minute for 30 minutes using a microplate reader (M200Pro, Tecan). Slope during linear decrease in absorption was calculated and directly corresponds to the amount of LDH leaked into cell culture medium. Triton X-100 (0.1%) lysates were used to quantify cellular LDH content. Percent of LDH leakage was quantified by dividing extracellular activity by the sum of extracellular and intracellular activity multiplied by 100.

Statistical analyses

Sample size (n) indicates the number of independent experiments performed. Statistical tests were performed using GraphPad Prism Version 5.04. qPCR data was visualized as a heatmap using ClustVis4 with centered rows and unit-variance scaling (Metsalu and Vilo, 2015).

3 Results

3.1 Culturing RPTEC/TERT1 in matrigel induces tubular morphology

A 3D environment with or without continuous flow supports morphological changes and organotypic functions, as was shown for many polarized cells including renal proximal tubule cells (Zhang et al., 2009). It was therefore hypothesized that 3-dimensional expansion of the culture (3D) of RPTEC/TERT1 cells into an extracellular matrix-like environment would result in tubular morphology and a higher degree of cellular differentiation when compared to cultures on plastic plates (2D) or on membrane inserts (referred to as 2.5D). The final 3D culture protocol starts with seeding RPTEC/TERT1 cells onto a layer of matrigel, followed by capping with another matrigel layer after allowing cells to attach (Fig. 1A). Under these conditions, cells could be successfully cultured in 96-well plates with medium renewal every two to three days. Already a few hours after seeding on matrigel, cells started to form branched, connected structures (Fig. 1B, day 0). Capping the cells with another layer of matrigel after 16 h was required to stabilize the structures (Fig. 1B, day 1). Within this matrigel sandwich, the cells formed 3D tubule-like structures that condensed during the first two weeks of culture (Fig. 1B, day 15). Branchings occurred every 200-1000 µm and tubule diameters varied between 20-50 µm. Note that due to differentiation and tightening of the cells, some branches were dissociated during maturation (Fig. 1B, arrows). Under these 3D culture conditions, tubule-like RPTEC/TERT1 could be maintained for up to 60 days without major morphological changes or overgrowth by proliferating cells. Since the tubules did not invade further into the matrigel but differentiated within the two matrigel layers, the 3D culture could be easily examined at different time points using a standard benchtop microscope (Fig. 1B). The metabolic activities of these RPTEC/TERT1 cultures were analyzed at every medium renewal by quantifying glucose consumption and lactate production (Fig. 1C). Neither parameter changed over the duration of the culture, suggestive of a non-proliferative, metabolically stable condition (Fig. 1C). The rate of lactate production of below 1 is indicative of a primarily oxidative glucose metabolism, thus supporting the notion that the matrigel sandwich culture system allowed for sufficient oxygen diffusion (Fig. 1D). LDH leakage was employed to assess cell death during the first 23 days of cultivation (Fig. 1E). After an initial peak of LDH leakage at the first timepoint – most likely resulting from unattached cells – the 3D culture showed no detectable cell death within the subsequent 3 weeks (Fig. 1E). In summary, culturing RPTEC/TERT1 cells in the matrigel sandwich induced a prominent change in cellular morphology from the typical carpet-like monolayer known from 2D cultures (Fig. 1B) to a stable network of tubular structures.

3.2 3D cultured RPTEC/TERT1 form a highly polarized epithelium

Further structural and phenotypic characterization of the tubular structures was achieved by confocal and electron microcopy. Using different optical planes, tubules were shown to consist of a single layer of RPTEC/TERT1 cells surrounding a lumen (Fig. 2A). The tubular lumen, already perceivable under bright field, was clearly delineated when using Hoechst 33342 to stain nuclei (Fig. 2A). A yz-projection revealed that nuclei are arranged in a circular manner, confirming the *in vivo* like morphotype (Fig. 2A, yz). Confocal microscopy of a branched structure is shown in Figure 2B. Using z-stack analyses, tubular diameters were found to range between ~20-50 µm, equaling ~2-5 cells (mean cellular diameter = 10µm). Next, the polarization of the 3D cultured RPTEC/TERT1 cells was assessed using immunocytochemical detection of typical proximal epithelial membrane markers. Antibodies for acetylated tubulin stain primary cilia and the tight junction protein zonula occludens protein 3 (ZO-3) was stained to investigate apical membrane local-

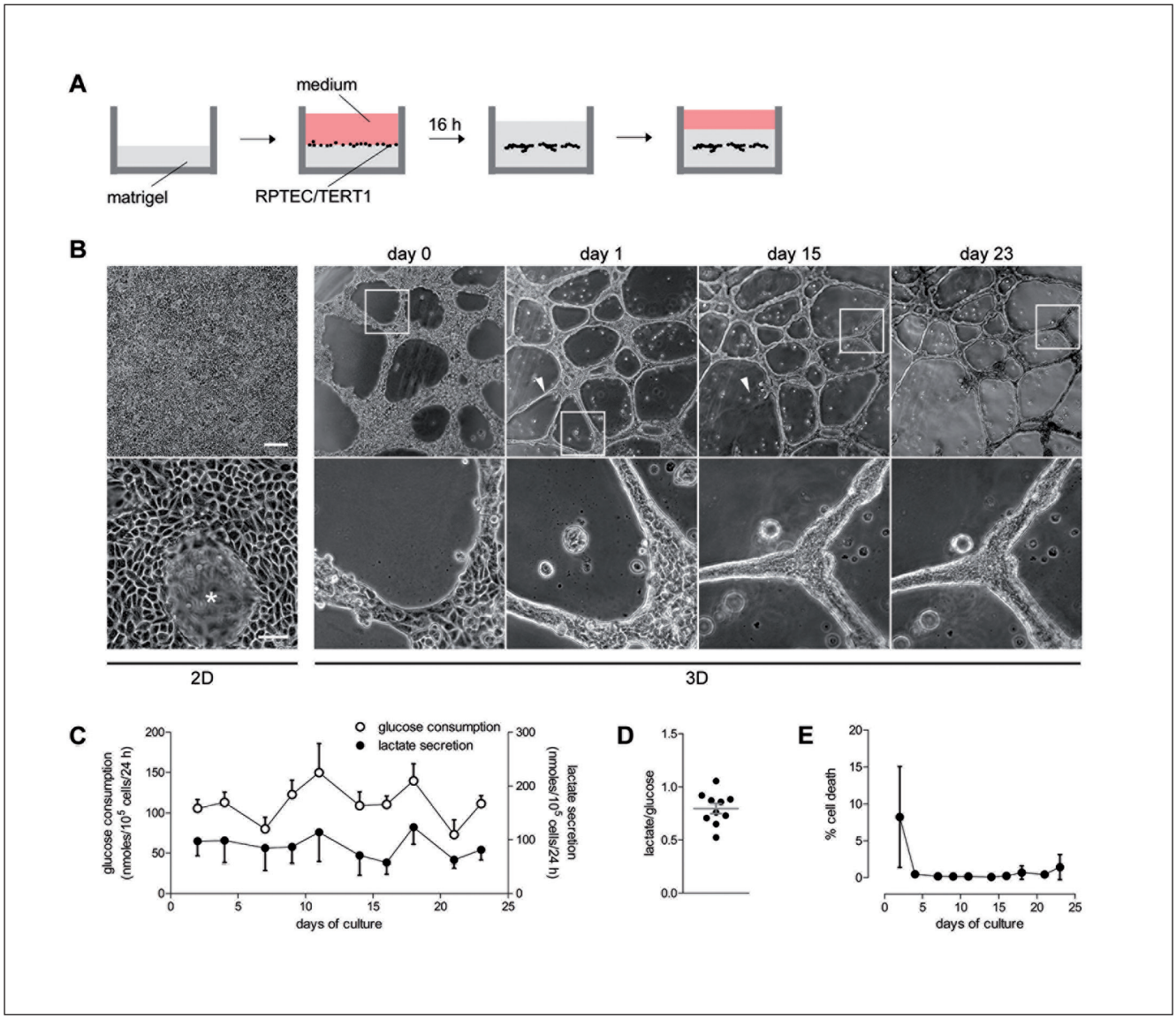

Fig. 1: RPTEC/TERT1 cells cultured in matrigel form stable tubular structures

A) Schematic illustration of the 3D culture of RPTEC/TERT1. Cells are seeded on top of a matrigel layer and form stable tubular structures within 16 h. Cells are then capped with another thin layer of matrigel and covered with culture medium. B) Bright-field microscopy of RPTEC/TERT1 grown either on plastic (2D) or in matrigel sandwich (3D). RPTEC/TERT1 grown on plastic (2D) form a dense monolayer including characteristic domes (*). When grown on matrigel coating (day 0), cells form branched tubular structures. Capping the cells with another matrigel layer (day 1) stabilizes cell morphology for at least 23 days. Arrow indicates dissociation of branches during maturation. Box indicates magnified area. Scale = 200 µm (upper panel), 50 µm (lower panel). C) Glucose consumption and lactate production measured in medium of 3D-cultures was stable for 23 days. Mean ± SEM, n = 6 with 20 technical replicates. D) Ratio of secreted lactate divided by consumed glucose. Each dot represents the mean of 6 replicates at each time point between day 2 and day 23. Lines indicate mean ± SEM. E) LDH leakage revealed absence of cell death for at least 23 days after initial attachment phase. Mean ± SD, n = 8 with 20 technical replicates.

ization (Fig. 2C, panel 1 + 2). Cilia formation was evidenced by positive staining of acetylated tubulin, which showed the expected luminal orientation (Fig. 2C, panel 1). Formation of apical tight-junctions was confirmed via ZO-3 staining (Fig. 2C, panel 2), while Na^+/K^+-ATPase was found localized at the basolateral surface of the tubular structures, as would be predicted from its localization *in vivo* (Fig. 2C, panel 3). Co-staining of ZO-3 and Na^+/K^+-ATPase corroborated the proper localization of the membrane markers as shown in Figure 2, panel 4. Transmission electron microcopy images,

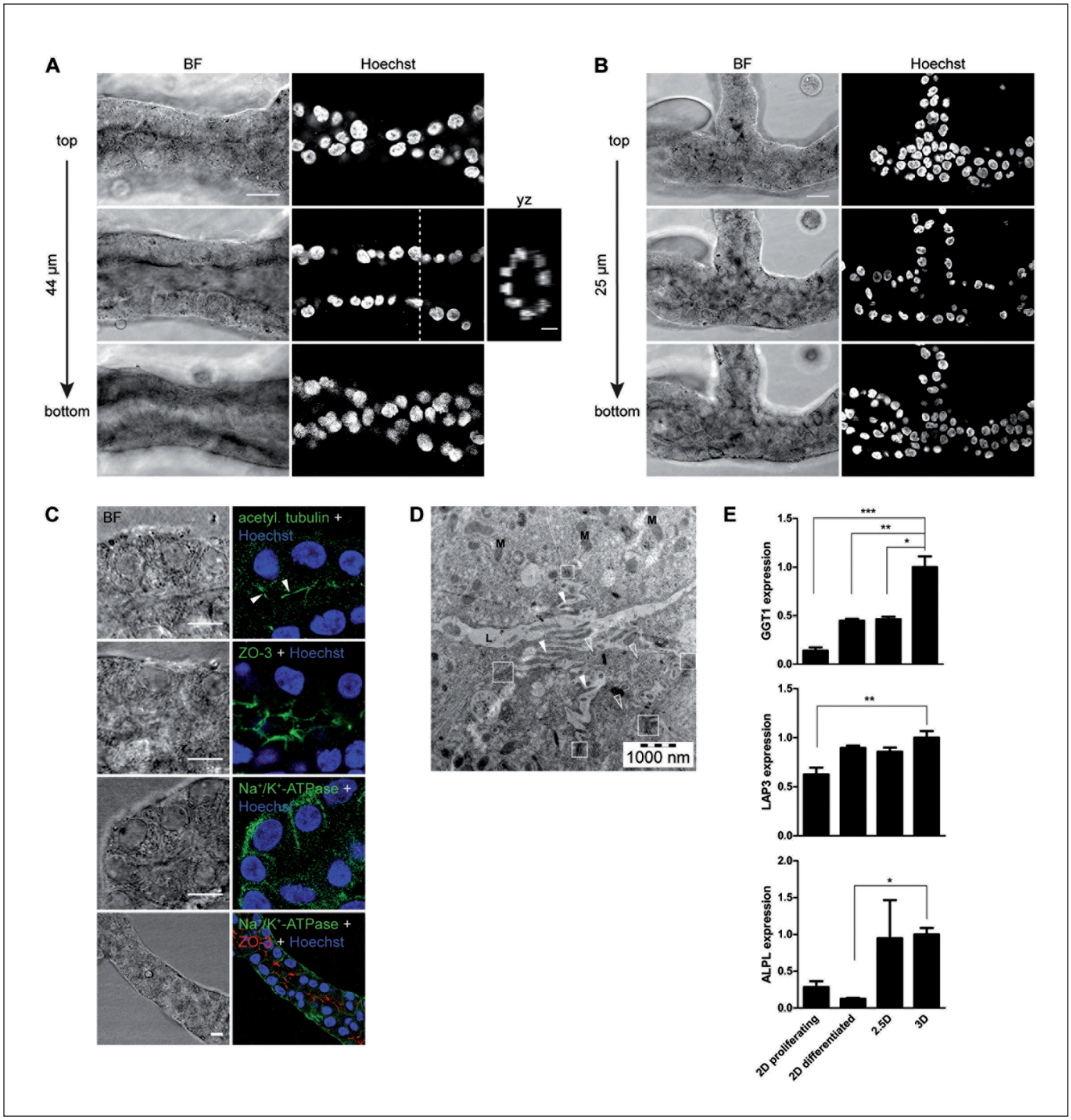

Fig. 2: Tubular structures of RPTEC/TERT1 cells contain highly polarized cells encircling a lumen

Confocal microscopy of a straight (A) and an intersected (B) 3D tubular structure. Cells form a single-layered tubule encircling a lumen. Dotted line indicates area of yz-projection. Scale = 20 µm. $Scale_{yz}$ = 10 µm. C) Immunocytochemistry showing luminal localization of cilia (acetylated tubulin, white arrow) and tight junctions (ZO-3) as well as basolateral localization of Na^+/K^+-ATPase. Co-staining of Na^+/K^+-ATPase (green) and ZO-3 (red) indicate polarization of cells within the tubule. Nuclei were stained with Hoechst (blue). Scale = 10 µm. D) Transmission electron microscopy of luminal area of 3D tubular structure. M = mitochondria, L = lumen, box = tight junction, arrow = microvilli (filled = longitudinal section, open = cross section). E) mRNA expression levels of apical brush border marker enzymes. Mean ± SEM, n = 4 with technical triplicates (2D and 2.5D); n = 10 with technical duplicates (3D). One-way ANOVA with Bonferroni's post-test. $p \leq 0.05$ (*), $p \leq 0.01$ (**), $p \leq 0.001$ (***). BF = bright field, 2D = grown on plastic, 2.5D = grown on transwell inserts, 3D = grown in matrigel sandwich, GGT1 = γ-glutamyltransferase 1, LAP3 = leucine aminopeptidase 3, ALPL = alkaline phosphatase.

showing columnar, prismatic cells with a pronounced apical brush border (arrows), a small lumen (L), mitochondria (M), and sub-apical tight junctions (boxes) (Fig. 2D), supported the *in vivo* like morphology of the tubular structures. Nuclei were oriented more towards the basolateral membrane (not shown). This highly differentiated, polarized and *in vivo* like phenotype of the 3D model was further supported by the enhanced expression of brush border markers, e.g., glutamyltransferase 1 (GGT1), leucine aminopeptidase (LAP3) and alkaline phosphatase (ALPL) when compared to cells cultured under simpler conditions (Fig. 2E).

Taken together, the 3D model demonstrated promising *in vivo*-like features, thus suggesting that the 3D approach enhances more profound differentiation and possibly functionality.

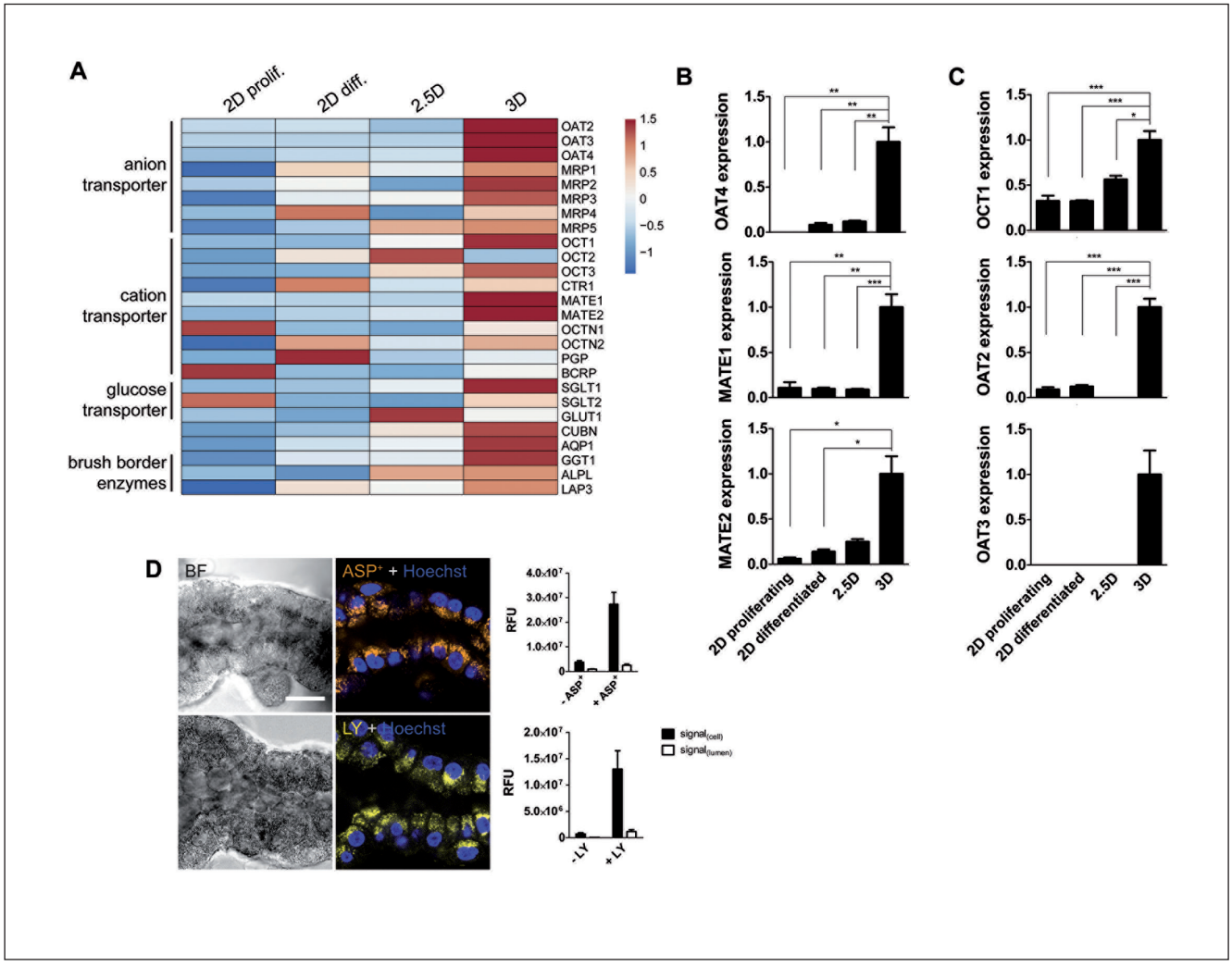

Fig. 3: Tubular structures exhibit increased transporter and membrane marker expression compared to 2D cultures
(A) Heat map of mRNA expression levels of 26 selected transporters and membrane markers under different culture conditions. (B) Exemplary graphs of apical transporters OAT4 and MATE1+2 expression under different culture conditions. (C) Exemplary graphs of basolateral transporters OCT1 and OAT2+3 expression. Mean ± SEM, n = 4 with technical triplicates (2D and 2.5D); n = 10 with technical duplicates (3D). One-way ANOVA with Bonferroni's post-test. $p \leq 0.05$ (*), $p \leq 0.01$ (**), $p \leq 0.001$ (***). Graphs for all other transporters are presented in Figure S1[1]. (D) Confocal microscopy of OCT substrate ASP^+ (upper panel) and OAT substrate LY (lower panel) uptake for 24 h into 3D grown cells. Nuclei were stained with Hoechst (blue). Signal intensity was quantified in cells and lumen of tubules stained with Hoechst only (- ASP^+/LY) or tubules exposed to ASP^+ or LY (+ ASP^+/LY). Mean ± SD, 15 regions of interest. 2D = grown on plastic, 2.5D = grown on transwell inserts, 3D = grown in matrigel sandwich, OAT = organic anion transporter, MRP = multidrug resistance protein, OCT = organic cation transporter, CTR1 = copper transporter 1, MATE = multidrug and toxin extrusion protein, OCTN = organic cation/carnitine transporter, PGP = multidrug resistance protein/p-glycoprotein, BCRP = breast cancer resistance protein, SGLT = sodium/glucose co-transporter, GLUT1 = glucose transporter 1, CUBN = cubilin, AQP1 = aquaporin 1, GGT1 = γ-glutamyltransferase 1, ALPL = alkaline phosphatase, LAP3 = leucine aminopeptidase 3, BF = bright field, RFU = relative fluorescence unit.

3.3 Induction of transporter expression in tubular structures

A common set-back of established renal proximal tubule cell models *in vitro* is the reduction or even loss of inherent transporter expression. Consequently, enhanced differentiation in a 3D model should also become manifest in a higher expression of functional entities, e.g., xenobiotic transporters. Therefore, the mRNA expression of multiple xenobiotic transporters, typically expressed in RPTECs, was compared in proliferating 2D and differentiated 2D, 2.5D, as well as 3D RPTEC/TERT1 cells (Fig. 3A). Overall, a striking increase in gene expression with differentiation status and, more importantly, with increasing complexity of culture conditions was observed, typically showing highest expression in the 3D culture system (Fig. 3A). Moreover, expression of OAT3 was exclusively observed under 3D culture conditions, commensurate with a higher expression level of OAT2 and 4 (Fig. 3B-C). Three members of the multidrug resistance protein (MRP) family, two of three tested organic cation uptake transporters (OCT) and both efflux transporters MATE1 and MATE2 also showed increased expression levels when compared to 2D or 2.5D culture conditions (Fig. 3A-C). Similarly, the expression level of typical renal proximal tubule transporters, e.g., cubilin (CUBN), sodium/glucose cotransporter (SGLT) 1 and aquaporin 1 (AQP1), as well as the brush border markers, GGT1, LAP3 and ALPL, increased with complexity of the culture conditions (Fig. 2E, Fig. 3A). Contrary to the general trend, several other transporters, including organic cation/carnitine transporter (OCTN) 1, OCTN2, P-gp, breast cancer resistance protein (BCRP) and SGLT2 and glucose transporter (GLUT) 1, did not show the highest expression level under 3D culture conditions (Fig. 3A).

In order to verify functionality of the organic anion and cation transporters, fluorescent probes, i.e., ASP^+ and Lucifer yellow (LY), were applied to the 3D tubules. The experiments demonstrated that these dyes were taken up into the cells but were not secreted into the lumen of the tubular structures, thus suggesting active anion and cation uptake but lack of efficient excretion (Fig. 3D). In contrast, cells grown in 2.5D were shown to exhibit vectorial transport for ASP^+ but not LY (data not shown).

Taken together, culturing RPTEC/TERT1 cells in a 3D matrix resulted in drastic changes in gene expression of several apical and basolateral transporters and marker enzymes including *de novo* expression of transporters which were so far absent in this cell line.

3.4 Application as nephrotoxicity model

For an initial sensitivity assessment, this novel 3D tubule model was challenged with the known nephrotoxicant cisplatin. Cisplatin is a chemotherapeutic used for treatment of various malignancies, e.g., lung or testis cancer, but dosing is limited by nephrotoxicity (Manohar and Leung, 2017). Cisplatin is actively taken up into RPTECs mainly via OCTs and copper transporter (CTR) 1 and intracellular accumulation is linked to DNA damage and mitochondrial dysfunction (Miller et al., 2010). Nephrotoxicity occurs in 20-35% of patients receiving cisplatin treatment (Hartmann et al., 1999; dos Santos et al., 2012), whereby the decline in renal function is typically observed several days after the single dose drug administration (Miller et al., 2010; Jang et al., 2013). To allow detection of this delayed manifestation of nephrotoxicity, differentiated RPTEC/TERT1 cells grown in 2D, 2.5D and 3D were exposed to 10, 50 and 100 µM cisplatin for 24 h. The lowest concentration mimicked that typically used in the clinical setting (Salas et al., 2006). Cell death was monitored via LDH release over the subsequent 10 days in the absence of cisplatin. Cell viability was determined on day 11 after initial 24 h exposure using resazurin reduction (Fig. 4A). Only 3D cultured cells demonstrated significantly impaired cell viability (60% of control) at the lowest cisplatin concentration (Fig. 4B). Superior sensitivity of the 3D cultured cells is observed despite the expression of the luminal cisplatin exporters MATE1 and MATE2 being significantly increased compared to the other culturing conditions (Fig. 3B). Although MATE activity is reported to protect from cisplatin toxicity (Nakamura et al., 2010), clearance of cisplatin into the tubular lumen via MATE may be impeded as was also observed for Asp^+ and LY (Fig. 3D). At 50 µM cisplatin, 2.5D and 3D cultured cells showed complete loss of viability, while 2D cultured cells appeared healthy. The highest concentration (100 µM) resulted in complete loss of viability at all culture conditions. The time-resolved quantification of cell death revealed absence of cytotoxicity during the exposure phase (24 h) of the experiment for all culture conditions and concentrations (Fig. 4C). Starting from day 3, however, 100 µM cisplatin provoked significant and persisting cell death at all culture conditions. The 50 µM concentration on the other hand caused persistent cell death only in 2.5D and 3D cultured cells, whereas in 2D cultures cell death was detectable on day 3 but not at later time-points. Thus, 2D cultured RPTEC/TERT1 cells appear capable to recover from the toxic insult of 50 µM cisplatin, as also supported by the viability measurements (Fig. 4B). Finally, at the clinically relevant concentration, cisplatin did not cause significant cell death in either culture condition. The latter suggested that the decrease of viability observed under 3D culture conditions (Fig. 4B) is not related to crude cell death but likely results from sustained and cumulative cell damage.

In conclusion, the 3D culture demonstrated a higher sensitivity toward delayed cisplatin nephrotoxicity than the 2.5D condition, which is often considered the gold standard for RPTEC culture (Aschauer et al., 2015a,b; Palmoski et al., 1992; Justice et al., 2009). Moreover, the capability of demonstrating delayed nephrotoxicity at clinically relevant concentrations of cisplatin is promising, especially with regard to *in vitro* to *in vivo* extrapolations.

4 Discussion

The renal proximal tubule plays a major role in maintaining the body's fluid, ion and glucose homeostasis. The underlying mechanisms of physiology and pathophysiology of proximal tubule cells are of key interest to researchers of many scientific areas. Since the proximal tubule is also a main target of drug-induced toxicity due to its role in drug transport and secretion, the detection of nephrotoxic lead compounds in nonclin-

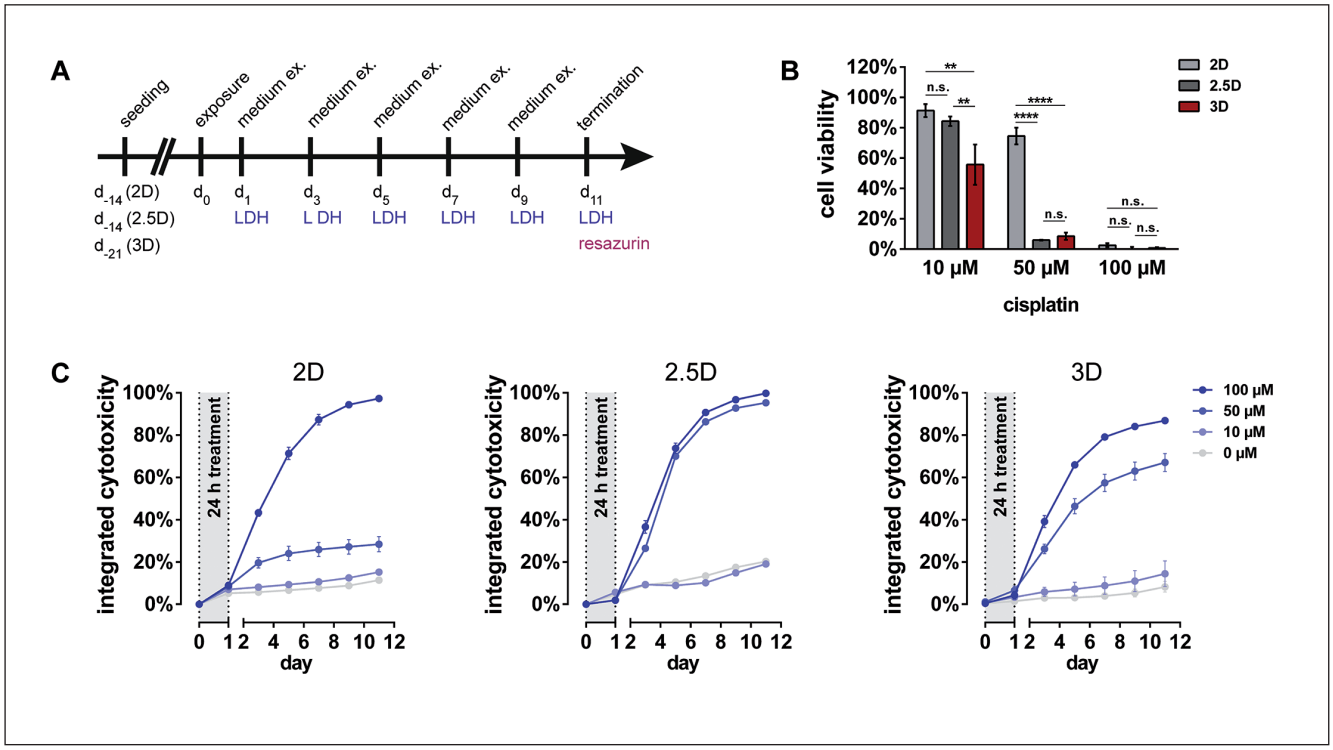

Fig. 4: 3D cultured RPTEC/TERT1 cells are sensitive towards delayed cisplatin toxicity

(A) Schematic of the experimental setup. RPTEC/TERT1 cells were cultured in 2D, 2.5D and 3D and exposed to cisplatin for 24 h. Cells remained in culture for the following 10 days with regular medium exchanges (medium ex.). LDH activity as a marker for cytotoxicity was quantified after every medium renewal. At day 11, cell viability was determined via resazurin reduction and cellular LDH content is quantified after cell lysis. (B) Cell viability of RPTEC/TERT1 cells cultured in the three different culture conditions after 24 h cisplatin exposure followed by cultivation for 10 days. Mean ± SEM, n = 3. Two-way ANOVA with Bonferroni's post-test. $p \leq 0.01$ (**); $p \leq 0.0001$ (****); n.s., not significant. (C) Integrated LDH leakage over the complete experimental duration. LDH activity was determined in cell culture medium after every medium renewal. Integrated LDH activities are presented as combined activities until respective time point and calculated relative to the complete activity (all supernatants plus lysate at day 11) and given as percent. Mean ± SEM, n = 4. 2D = grown on plastic, 2.5D = grown on transwell inserts, 3D = grown in matrigel sandwich, LDH = lactate dehydrogenase.

ical trials remains particularly important. Due to interspecies variability, animal models have only limited predictivity for human nephrotoxicity (Astashkina et al., 2012a) while validated human *in vitro* test systems are still missing (Tiong et al., 2014). The inability to predict drug-induced kidney injury early during pharmacological development is illustrated by the fact that nephrotoxicity accounts for only 2% and 5% of drug attrition in nonclinical and phase I studies (Redfern et al., 2010), respectively, while unexpected toxicity, including nephrotoxicity, accounts for approximately 30% of drug attrition in the clinic (Kola and Landis, 2004). Reliable nonclinical detection would therefore allow rapid cancellation of nephrotoxic drug candidates resulting in huge savings in cost and time and, more importantly, could prevent harmful events in patients. Interestingly, the ability to detect nephrotoxicity *in vitro* appears primarily dependent on the differentiation status of the cell used rather than on the endpoint selected (Tiong et al., 2014). Moreover, most *in vitro* tests appear to be running with rather undifferentiated cells while fully differentiated proximal tubule cell systems are still missing.

The culture model with RPTEC/TERT1 cells presented here allowed for tubular structure formation similar to the *in vivo* situation. RPTEC/TERT1 have been shown to express a variety of drug transporters and can be cultured as a differentiated monolayer for extended time periods (Wieser et al., 2008; Aschauer et al., 2015a, 2013). Still, transporter expression levels are markedly lower when compared to *in vivo* data and both expression and functionality of organic anion transporters (OATs) remain controversial (Aschauer et al., 2015a). However, it was hypothesized that improved differentiation could be achieved when RPTEC/TERT1 are cultured in a 3D matrix. Indeed, solely providing RPTEC/TERT1 with a suitable extracellular matrix was sufficient to induce the development of *in vivo*-like proximal tubules without need of additional growth factors or cytokines. The sandwich culture method allowed for simple microscopic analyses since tubular structures form within one layer and morphology therefore can be easily monitored using bright-field microscopy. Moreover, these *in vivo*-like proximal tubules were demonstrated to be highly stable and viable for up to 60 days as shown via glucose uptake, lactate secretion and cell death

measurements during long-term culture. Despite pronounced proliferation and cell death not being observed in the tubular structures, a low rate of cellular turnover and replacement as occurs under physiological conditions *in vivo* cannot be excluded. If cellular replacement occurs within this 3D model, it could also serve as a new *in vitro* tool for detecting and investigating mechanisms of renal carcinogenesis promoted by increased rates of degenerative/regenerative proliferation.

The overall increase in expression of transporters, more explicitly the *de novo* expression of OAT3, as well as the correct cellular polarization and organization (e.g., tight junction formation), is testimony of the improved differentiation status of RPTEC/TERT1 in the matrigel sandwich. Partial proof of physiologic functionality was obtained by investigating the basolateral to apical transport using Asp^+ and LY. Although uptake was demonstrated, excretion, and thus true vectorial transport, was not observed. Indeed, contrary to other studies (Masereeuw et al., 1999; Han et al., 2004; Freedman et al., 2015) and expectations, Asp^+ and LY were not secreted into the tubular lumen. One of the missing factors in the 3D model presented here is a continuous flow of a primary urine equivalent, known to trigger widening of the inner and outer diameter of proximal tubules (Raghavan and Weisz, 2016; Du et al., 2006) and thus providing for a functional lumen. Therefore, it appears likely that the absence of flow reduces both the tubular diameter and the capacity to excrete substrates into the lumen of the tubules in the 3D model presented here. Irrespective of the latter, the 3D model demonstrated enhanced sensitivity toward cisplatin, a model nephrotoxicant. Moreover, the 3D model allowed detection of nephrotoxicity at a clinically relevant concentration and setting (one-time bolus dose of 10 µM). In addition, the high stability and viability of this model would also support mechanistic investigation of the sustained and cumulative cell damage observed. The latter is an encouraging finding that could trigger future studies aiming to assess the usefulness of this model for detection of drug-induced nephrotoxicity.

To date, several cell types have been reported to form tubule-like structures when cultured in extracellular matrices, e.g., matrigel (Niemann et al., 1998; Debnath et al., 2002; Hadley et al., 1990). Moreover, there is data on 3D culture of primary rabbit (Han et al., 2004), primary human proximal tubule cells (DesRochers et al., 2013), murine proximal tubule fragments (Astashkina et al., 2012b) and, very recently, the RPTEC/TERT1 cell line (Homan et al., 2016). Using primary cells has the disadvantage of a limited cell source subject to inter-donor variability. While the inter-donor variability of primary human cells can represent a desired feature to investigate the relevance of genetic variations for toxicity, it is often considered disadvantageous in routine testing. Thus, using immortalized cells, e.g., RPTEC/TERT1, provides for the advantage of a continuous and well-defined source and thus higher reproducibility. Homan et al. used bioprinted 3D proximal tubules on a chip populated with RPTEC/TERT1 cells, allowing also the formation of a differentiated and polar epithelium, while including flow and thus shear stress known to be beneficial for RPTEC differentiation (Jang et al., 2013). The latter system, while similar to the 3D model presented here, is much more complex and technically demanding, thus not allowing simple transfer and establishment in any standard cell culture laboratory. Moreover, while RPTEC/TERT1 cells in the 3D model presented here assembled to tubular structures autonomously, this is not the case in the tubule-on-a-chip system of Homan et al., where cells are seeded onto a printed scaffold. Whether or not the chip-system by Homan et al. displays similar sensitivity towards cisplatin as the easy-to-use 3D model described here cannot be ascertained as missing data on cisplatin toxicity prevents a direct comparison and thus remains to be determined.

Taken together, the RPTEC/TERT1 3D culture model presented here showed morphological and functional similarity to human kidney proximal tubules *in vivo*. Culturing RPTEC/TERT1 cells in a matrigel sandwich induced tubule formation and further increased differentiation specifically with regard to polarity and transporter expression when compared to classic 2D or 2.5D cultures on transwell inserts. The easy-to-use model described here may prove to be useful for mechanistic investigations, e.g., in discovery of compounds interfering with tubule formation, differentiation and polarization, as well for the detection and understanding of pharmaceutical induced nephrotoxicity.

References

Alépée, N., Bahinski, A., Daneshian, M. et al. (2014). State-of-the-art of 3D cultures (organs-on-a-chip) in safety testing and pathophysiology. *ALTEX 31*, 441-477. doi:10.14573/altex1406111

Aschauer, L., Gruber, L. N., Pfaller, W. et al. (2013). Delineation of the key aspects in the regulation of epithelial monolayer formation. *Mol Cell Biol 33*, 2535-2550. doi:10.1128/MCB.01435-12

Aschauer, L., Carta, G., Vogelsang, N. et al. (2015a). Expression of xenobiotic transporters in the human renal proximal tubule cell line RPTEC/TERT1. *Toxicol In Vitro 30*, 95-105. doi:10.1016/j.tiv.2014.12.003

Aschauer, L., Limonciel, A., Wilmes, A. et al. (2015b). Application of RPTEC/TERT1 cells for investigation of repeat dose nephrotoxicity: A transcriptomic study. *Toxicol In Vitro 30*, 106-116. doi:10.1016/j.tiv.2014.10.005

Astashkina, A., Mann, B. and Grainger, D. W. (2012a). A critical evaluation of in vitro cell culture models for high-throughput drug screening and toxicity. *Pharmacol Ther 134*, 82-106. doi:10.1016/j.pharmthera.2012.01.001

Astashkina, A. I., Mann, B. K., Prestwich, G. D. et al. (2012b). A 3-D organoid kidney culture model engineered for high-throughput nephrotoxicity assays. *Biomaterials 33*, 4700-4711. doi:10.1016/j.biomaterials.2012.02.063

Biermann, J., Lang, D., Gorboulev, V. et al. (2006). Characterization of regulatory mechanisms and states of human organic cation transporter 2. *Am J Physiol Cell Physiol 290*, C1521-1531. doi:10.1152/ajpcell.00622.2005

Bissell, M. J., Radisky, D. C., Rizki, A. et al. (2002). The organizing principle: Microenvironmental influences in the

normal and malignant breast. *Differentiation 70*, 537-546. doi:10.1046/j.1432-0436.2002.700907.x

Bunnage, M. E. (2011). Getting pharmaceutical R&D back on target. *Nat Chem Biol 7*, 335-339. doi:10.1038/nchembio.581

Cetinkaya, I., Ciarimboli, G., Yalcinkaya, G. et al. (2003). Regulation of human organic cation transporter hOCT2 by PKA, PI3K, and calmodulin-dependent kinases. *Am J Physiol Renal Physiol 284*, F293-302. doi:10.1152/ajprenal.00251.2002

Debnath, J., Mills, K. R., Collins, N. L. et al. (2002). The role of apoptosis in creating and maintaining luminal space within normal and oncogene-expressing mammary acini. *Cell 111*, 29-40. doi:10.1016/S0092-8674(02)01001-2

DesRochers, T. M., Suter, L., Roth, A. et al. (2013). Bioengineered 3D human kidney tissue, a platform for the determination of nephrotoxicity. *PLoS One 8*, e59219. doi:10.1371/journal.pone.0059219

dos Santos, N. A., Carvalho Rodrigues, M. A., Martins, N. M. et al. (2012). Cisplatin-induced nephrotoxicity and targets of nephroprotection: An update. *Arch Toxicol 86*, 1233-1250. doi:10.1007/s00204-012-0821-7

Du, Z., Yan, Q., Duan, Y. et al. (2006). Axial flow modulates proximal tubule NHE3 and H-ATPase activities by changing microvillus bending moments. *Am J Physiol Renal Physiol 290*, F289-296. doi:10.1152/ajprenal.00255.2005

Dunn, J. C., Tompkins, R. G. and Yarmush, M. L. (1991). Long-term in vitro function of adult hepatocytes in a collagen sandwich configuration. *Biotechnol Prog 7*, 237-245. doi:10.1021/bp00009a007

Freedman, B. S., Brooks, C. R., Lam, A. Q. et al. (2015). Modelling kidney disease with CRISPR-mutant kidney organoids derived from human pluripotent epiblast spheroids. *Nat Commun 6*, 8715. doi:10.1038/ncomms9715

Grabinger, T., Luks, L., Kostadinova, F. et al. (2014). Ex vivo culture of intestinal crypt organoids as a model system for assessing cell death induction in intestinal epithelial cells and enteropathy. *Cell Death Dis 5*, e1228. doi:10.1038/cddis.2014.183

Hackam, D. G. and Redelmeier, D. A. (2006). Translation of research evidence from animals to humans. *JAMA 296*, 1731-1732. doi:10.1001/jama.296.14.1731

Hadley, M. A., Weeks, B. S., Kleinman, H. K. et al. (1990). Laminin promotes formation of cord-like structures by Sertoli cells in vitro. *Dev Biol 140*, 318-327. doi:10.1016/0012-1606(90)90082-T

Han, H. J., Sigurdson, W. J., Nickerson, P. A. et al. (2004). Both mitogen activated protein kinase and the mammalian target of rapamycin modulate the development of functional renal proximal tubules in matrigel. *J Cell Sci 117*, 1821-1833. doi:10.1242/jcs.01020

Hartmann, J. T., Kollmannsberger, C., Kanz, L. et al. (1999). Platinum organ toxicity and possible prevention in patients with testicular cancer. *Int J Cancer 83*, 866-869. doi:10.1002/(SICI)1097-0215(19991210)83:6<866::AID-IJC34>3.0.CO;2-9

Hartung, T. (2009). Toxicology for the twenty-first century. *Nature 460*, 208-212. doi:10.1038/460208a

Heussner, A. H. and Dietrich, D. R. (2013). Primary porcine proximal tubular cells as an alternative to human primary renal cells in vitro: An initial characterization. *BMC Cell Biol 14*, 55. doi:10.1186/1471-2121-14-55

Homan, K. A., Kolesky, D. B., Skylar-Scott, M. A. et al. (2016). Bioprinting of 3D convoluted renal proximal tubules on perfusable chips. *Sci Rep 6*, 34845. doi:10.1038/srep34845

Itoh, M., Umegaki-Arao, N., Guo, Z. et al. (2013). Generation of 3D skin equivalents fully reconstituted from human induced pluripotent stem cells (iPSCS). *PLoS One 8*, e77673. doi:10.1371/journal.pone.0077673

Jang, K. J., Mehr, A. P., Hamilton, G. A. et al. (2013). Human kidney proximal tubule-on-a-chip for drug transport and nephrotoxicity assessment. *Integr Biol (Camb) 5*, 1119-1129. doi:10.1039/c3ib40049b

Justice, B. A., Badr, N. A. and Felder, R. A. (2009). 3D cell culture opens new dimensions in cell-based assays. *Drug Discov Today 14*, 102-107. doi:10.1016/j.drudis.2008.11.006

Kola, I. and Landis, J. (2004). Can the pharmaceutical industry reduce attrition rates? *Nat Rev Drug Discov 3*, 711-715. doi:10.1038/nrd1470

Lee, G. Y., Kenny, P. A., Lee, E. H. et al. (2007). Three-dimensional culture models of normal and malignant breast epithelial cells. *Nat Methods 4*, 359-365. doi:10.1038/nmeth1015

Leist, M. and Hartung, T. (2013). Inflammatory findings on species extrapolations: Humans are definitely no 70-kg mice. *Arch Toxicol 87*, 563-567. doi:10.1007/s00204-013-1038-0

Limonciel, A., Aschauer, L., Wilmes, A. et al. (2011). Lactate is an ideal non-invasive marker for evaluating temporal alterations in cell stress and toxicity in repeat dose testing regimes. *Toxicol In Vitro 25*, 1855-1862. doi:10.1016/j.tiv.2011.05.018

Lin, Z. and Will, Y. (2012). Evaluation of drugs with specific organ toxicities in organ-specific cell lines. *Toxicol Sci 126*, 114-127. doi:10.1093/toxsci/kfr339

Lu, H. F., Lim, S. X., Leong, M. F. et al. (2012). Efficient neuronal differentiation and maturation of human pluripotent stem cells encapsulated in 3D microfibrous scaffolds. *Biomaterials 33*, 9179-9187. doi:10.1016/j.biomaterials.2012.09.006

Manohar, S. and Leung, N. (2017). Cisplatin nephrotoxicity: A review of the literature. *J Nephrol 31,* 15-25. doi:10.1007/s40620-017-0392-z

Masereeuw, R., Moons, M. M., Toomey, B. H. et al. (1999). Active lucifer yellow secretion in renal proximal tubule: Evidence for organic anion transport system crossover. *J Pharmacol Exp Ther 289*, 1104-1111.

Matthews, R. A. (2008). Medical progress depends on animal models – Doesn't it? *J R Soc Med 101*, 95-98. doi:10.1258/jrsm.2007.070164

Metsalu, T. and Vilo, J. (2015). Clustvis: A web tool for visualizing clustering of multivariate data using principal component analysis and heatmap. *Nucleic Acids Res 43*, W566-570. doi:10.1093/nar/gkv468

Miller, R. P., Tadagavadi, R. K., Ramesh, G. et al. (2010). Mechanisms of cisplatin nephrotoxicity. *Toxins (Basel) 2*, 2490-2518. doi:10.3390/toxins2112490

Morrissey, K. M., Stocker, S. L., Wittwer, M. B. et al. (2013). Renal transporters in drug development. *Annu Rev Pharmacol Toxicol 53*, 503-529. doi:10.1146/annurev-pharmtox-011112-140317

Nakamura, T., Yonezawa, A., Hashimoto, S. et al. (2010). Disruption of multidrug and toxin extrusion MATE1 potentiates cisplatin-induced nephrotoxicity. *Biochem Pharmacol 80*, 1762-1767. doi:10.1016/j.bcp.2010.08.019

Niemann, C., Brinkmann, V., Spitzer, E. et al. (1998). Reconstitution of mammary gland development in vitro: Requirement of c-met and c-erbB2 signaling for branching and alveolar morphogenesis. *J Cell Biol 143*, 533-545. doi:10.1083/jcb.143.2.533

Olson, H., Betton, G., Robinson, D. et al. (2000). Concordance of the toxicity of pharmaceuticals in humans and in animals. *Regul Toxicol Pharmacol 32*, 56-67. doi:10.1006/rtph.2000.1399

Palmoski, M. J., Masters, B. A., Flint, O. P. et al. (1992). Characterization of rabbit primary proximal tubule kidney cell cultures grown on Millicell-HA membrane filters. *Toxicol In Vitro 6*, 557-567. doi:10.1016/0887-2333(92)90068-3

Raghavan, V. and Weisz, O. A. (2016). Discerning the role of mechanosensors in regulating proximal tubule function. *Am J Physiol Renal Physiol 310*, F1-5. doi:10.1152/ajprenal.00373.2015

Redfern, W. S., Ewart, L., Hammond, T. G. et al. (2010). Impact and frequency of different toxicities throughout the pharmaceutical life cycle. *The Toxicologist 114*, 231.

Roguet, R., Cohen, C., Dossou, K. G. et al. (1994). Episkin, a reconstituted human epidermis for assessing in vitro the irritancy of topically applied compounds. *Toxicol In Vitro 8*, 283-291. doi:10.1016/0887-2333(94)90195-3

Russell, W. M. S. and Burch, R. L. (1959). *The Principles of Humane Experimental Technique*. London, UK: Methuen & Co. Ltd. http://altweb.jhsph.edu/pubs/books/humane_exp/het-toc

Salas, S., Mercier, C., Ciccolini, J. et al. (2006). Therapeutic drug monitoring for dose individualization of cisplatin in testicular cancer patients based upon total platinum measurement in plasma. *Ther Drug Monit 28*, 532-539. doi:10.1097/00007691-200608000-00008

Sato, T., Vries, R. G., Snippert, H. J. et al. (2009). Single Lgr5 stem cells build crypt-villus structures in vitro without a mesenchymal niche. *Nature 459*, 262-265. doi:10.1038/nature07935

Sauzay, C., White-Koning, M., Hennebelle, I. et al. (2016). Inhibition of OCT2, MATE1 and MATE2-K as a possible mechanism of drug interaction between pazopanib and cisplatin. *Pharmacol Res 110*, 89-95. doi:10.1016/j.phrs.2016.05.012

Smirnova, L., Harris, G., Delp, J. et al. (2016). A luhmes 3D dopaminergic neuronal model for neurotoxicity testing allowing long-term exposure and cellular resilience analysis. *Arch Toxicol 90*, 2725-2743. doi:10.1007/s00204-015-1637-z

Tiong, H. Y., Huang, P., Xiong, S. et al. (2014). Drug-induced nephrotoxicity: Clinical impact and preclinical in vitro models. *Mol Pharm 11*, 1933-1948. doi:10.1021/mp400720w

Tostões, R. M., Leite, S. B., Miranda, J. P. et al. (2011). Perfusion of 3D encapsulated hepatocytes – A synergistic effect enhancing long-term functionality in bioreactors. *Biotechnol Bioeng 108*, 41-49. doi:10.1002/bit.22920

Tuschl, G., Hrach, J., Walter, Y. et al. (2009). Serum-free collagen sandwich cultures of adult rat hepatocytes maintain liver-like properties long term: A valuable model for in vitro toxicity and drug-drug interaction studies. *Chem Biol Interact 181*, 124-137. doi:10.1016/j.cbi.2009.05.015

van der Worp, H. B., Howells, D. W., Sena, E. S. et al. (2010). Can animal models of disease reliably inform human studies? *PLoS Med 7*, e1000245. doi:10.1371/journal.pmed.1000245

Wieser, M., Stadler, G., Jennings, P. et al. (2008). hTERT alone immortalizes epithelial cells of renal proximal tubules without changing their functional characteristics. *Am J Physiol Renal Physiol 295*, F1365-1375. doi:10.1152/ajprenal.90405.2008

Wilmer, M. J., Ng, C. P., Lanz, H. L. et al. (2016). Kidney-on-a-chip technology for drug-induced nephrotoxicity screening. *Trends Biotechnol 34*, 156-170. doi:10.1016/j.tibtech.2015.11.001

Zeilinger, K., Schreiter, T., Darnell, M. et al. (2011). Scaling down of a clinical three-dimensional perfusion multicompartment hollow fiber liver bioreactor developed for extracorporeal liver support to an analytical scale device useful for hepatic pharmacological in vitro studies. *Tissue Eng Part C Methods 17*, 549-556. doi:10.1089/ten.TEC.2010.0580

Zhang, H., Tasnim, F., Ying, J. Y. et al. (2009). The impact of extracellular matrix coatings on the performance of human renal cells applied in bioartificial kidneys. *Biomaterials 30*, 2899-2911. doi:10.1016/j.biomaterials.2009.01.046

Conflict of interest

The authors declare no conflict of interest.

Acknowledgements

We thank the Bioimaging Center (University of Konstanz) for providing the imaging equipment and support and the Electron Microscopy Center (University of Konstanz) for performing electron microscopy. This work was supported with a research grant (#15958812) from Boehringer-Ingelheim.

Correspondence to

Daniel R. Dietrich, PhD
Human and Environmental Toxicology
Department of Biology
University of Konstanz
Konstanz, Germany
e-mail: daniel.dietrich@uni-konstanz.de
https://orcid.org/0000-0003-0416-3811